JACS
JOURNAL OF THE AMERICAN CHEMICAL SOCIETY

pubs.acs.org/JACS

Article

Folding of an Intrinsically Disordered Iron-Binding Peptide in Response to Sedimentation Revealed by Cryo-EM

Geula Davidov,[⊥] Gili Abelya,[⊥] Ran Zalk, Benjamin Izbicki, Sharon Shaibi, Lior Spektor, Dayana Shagidov, Esther G. Meyron-Holtz, Raz Zarivach, and Gabriel A. Frank*

Cite This: *J. Am. Chem. Soc.* 2020, 142, 19551−19557

Read Online

ACCESS | Metrics & More | Article Recommendations | Supporting Information

ABSTRACT: Biomineralization is mediated by specialized proteins that guide and control mineral sedimentation. In many cases, the active regions of these biomineralization proteins are intrinsically disordered. High-resolution structures of these proteins while they interact with minerals are essential for understanding biomineralization processes and the function of intrinsically disordered proteins (IDPs). Here we used the cavity of ferritin as a nanoreactor where the interaction between M6A, an intrinsically disordered iron-binding domain, and an iron oxide particle was visualized at high resolution by cryo-EM. Taking advantage of the differences in the electron-dose sensitivity of the protein and the iron oxide particles, we developed a method to determine the irregular shape of the particles found in our density maps. We found that the folding of M6A correlates with the detection of mineral particles in its vicinity. M6A interacts with the iron oxide particles through its C-terminal side, resulting in the stabilization of a helix at its N-terminal side. The stabilization of the helix at a region that is not in direct contact with the iron oxide particle demonstrates the ability of IDPs to respond to signals from their surroundings by conformational changes. These findings provide the first glimpse toward the long-suspected mechanism for biomineralization protein control over mineral microstructure, where unstructured regions of these proteins become more ordered in response to their interaction with the nascent mineral particles.

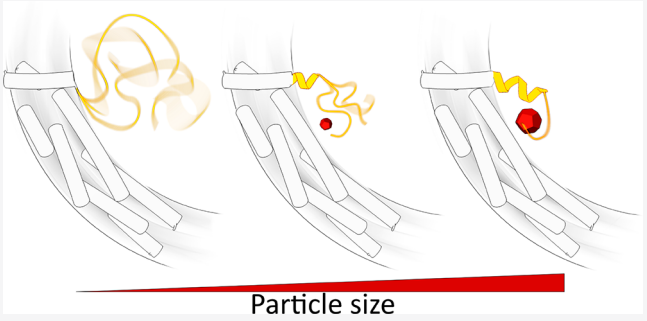

INTRODUCTION

Biomineralization is required for numerous biological processes, such as the formation of bones and shells, the regulation of ion concentrations, and the formation of magnetic minerals in magneto-sensing organs.[1,2] Organisms have exquisite control over the types and morphologies of the minerals they sediment. This control over the microstructure is mediated by a large group of highly specialized biomineralization proteins. To understand the molecular-level regulation of biomineralization processes, high-resolution structures of these protein−mineral complexes at different stages of biomineralization are required. However, there are only a handful of experimentally determined structures showing protein−biomineral complexes, typically consisting of only a few (3−8) metal ions.[3−5] In many cases, the functional regions of biomineralizing proteins are highly charged and intrinsically disordered.[6,7]

Direct structural observations of the formation of ordered structures induced by the interaction with sediments are still limited. While the structural changes in intrinsically disordered proteins (IDPs) upon interaction with proteins are well characterized,[8] similar effects as a result of interactions with minerals were mostly deduced from molecular dynamics simulations and spectroscopic measurements.[9,10] The interaction between IDPs and minerals is especially intriguing due to the binding promiscuity required for recognizing the surfaces of minerals with diverse sizes and shapes. Visualizing the ordering of IDPs upon their interaction with minerals will provide direct evidence for folding upon binding in biomineralization processes and shed light on the functional role of this effect.

Mms6 is a biomineralization protein, which aids in the formation of magnetite in the magnetotactic bacteria *Magnetospirillum magneticum* AMB-1. Mms6 is a protein with 133 amino acids that is predicted to have an N-terminal hydrophobic helix anchoring it to the magnetosome's membrane and a highly acidic C-terminal active segment (M6A) that nucleates and interacts with the magnetite.[11−16] Consistent with its highly hydrophilic and negatively charged sequence, M6A is intrinsically disordered and has a high affinity to ferrous ions.[15,17] While the interactions of M6A with the iron ions affect its 3D

Received: July 14, 2020
Published: November 9, 2020

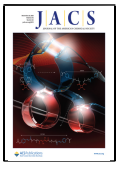

organization and dynamics, they do not lead to the stabilization of its structure.[15−17] Similarly, the structure of self-assembled micelles of Mms6 is modulated by adding a ferric or ferrous ion mix.[14] However, a higher resolution structure determination of Mms6 in this micellar form is challenging.[18] It was suggested that the main function of Mms6 is to facilitate the nucleation of magnetite nanocrystals, which are an essential part of the magnetosome.[15] However, it is unknown how M6A, the Mms6 iron-binding domain, and the forming biomineral interact and affect each other.

To test how M6A and the nascent biomineral particle affect each other, we looked for a way to bring a single M6A chain and a nanometer-scale iron oxide particle to close proximity under conditions that would allow for the structure determination. To do so, we developed a novel experimental strategy where M6A is conjugated to the C-terminus of L-ferritin (Figure 1).

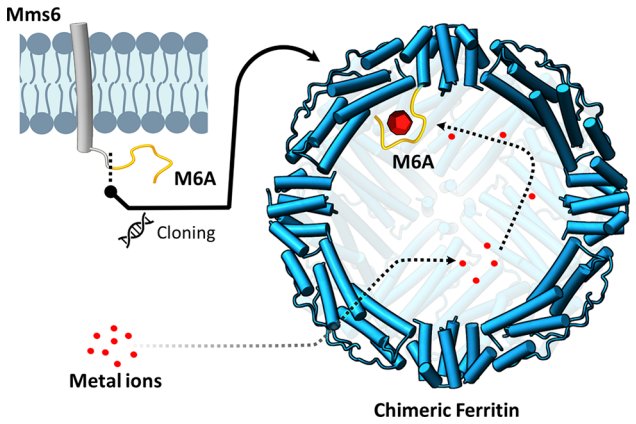

Figure 1. Using ferritin as a nanoreactor for probing the interaction between proteins and forming minerals. An active segment of the biomineralization protein (yellow) is expressed at the C-terminus of L-ferritin (blue). Upon metal uptake by the ferritin, minerals (red) are formed inside its cavity, and the interaction between the minerals and the biomineralization protein can be analyzed. Only a single functional loop and a single mineral are presented here for clarity.

Ferritins are arranged as a 24-subunit hollow nanocage enclosing a volume of ∼240 nm^3, large enough to harbor ∼4500 metal atoms as well as small molecules and peptides.[19,20] For their robust structure and high symmetry, ferritins became a staple of cryo-EM targets.[21] In vertebrates, L-ferritin is responsible for the nucleation of iron oxide within the hetero-oligomeric (L and H) ferritin assembly. When soaked in a solution of Fe^{2+} ions, uniform-size iron oxide atomic clusters consisting of several Fe ions nucleate inside L-ferritin.[4] This phenomenon was used to determine the interaction between the inner surface of L-ferritin and the iron oxide by X-ray crystallography.[4,5] Building on L-ferritin's ability to nucleate iron oxide, we set out to use it as a reaction vessel that could provide the local environment for studying the interaction of M6A with *in situ*-generated iron oxide nanoparticles while enabling the structure determination.

Here we report on the structural transformations of M6A in response to its interaction with nascent biomineral particles. Using our unique experimental strategy in combination with cryo-EM and X-ray crystallography, we observed structural changes in M6A from a disordered state in the absence of mineral deposits to a stable helix and an extended loop that strongly interacts with an iron oxide particle. Between these two extreme conditions, in the vicinity of a smaller iron oxide deposit we found M6A in a partially structured state where part of the helix was formed but the extended loop was still disordered.

RESULTS

The X-ray structure of H-ferritin-M6A was previously determined,[20] and it was demonstrated that ferritin's C-terminus, where M6A is conjugated, is inside the nanocage. In this construct, M6A can potentially interact with the iron ions that enter the ferritin nanocage. However, M6A was not resolved by the H-ferritin-M6A X-ray structure. To examine the molecular details of the interaction between a forming biomineral and M6A, we cloned it into the C-terminus of mouse L-ferritin behind a glycine spacer (Figure 1). The structure of the purified chimeric protein was then solved using cryo-EM and X-ray crystallography under various conditions.

To monitor the effect of the ferritin scaffold on M6A, we determined the structure of L-ferritin-M6A after purification (the "untreated" sample), using cryo-EM (Figure 2). In this

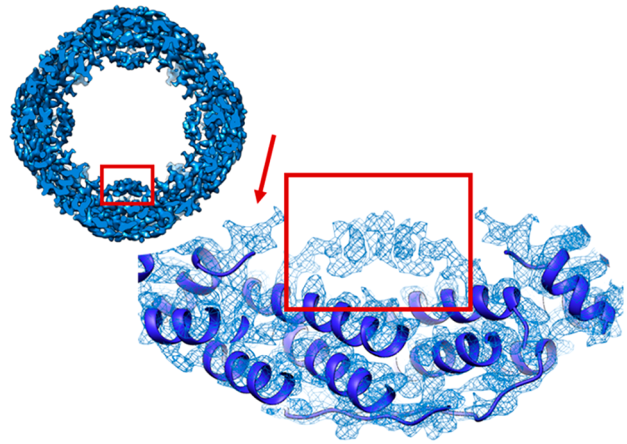

Figure 2. M6A becomes partially structured in the presence of a biomineral particle. A cut through the EM density map (top left) reveals the formation of the biomineral particles in the cavity of ferritin (red box). The ribbon model of mouse L-ferritin (PDB 1LB3[24]), fitted to the map presented as a wireframe, is depicted at the bottom. The extra helical turn and the extra density found in the untreated sample are marked by an arrow and a box, respectively.

∼3.4 Å resolution structure, roughly spherical densities are attached to the inner surface of ferritin at the suggested L-ferritin ferrihydrite nucleation site,[4] which is consistent with the formation of biomineral particles. As indicated by its elution volume during size exclusion chromatography (SEC), L-ferritin-M6A was purified as a 24-mer nanocage assembly. Given that the buffers used during purification had no iron (or other transition metals), it is likely that the mineral particles were formed *in vivo* and not during the purification process (Figure S1), supporting the notion that this extra density is likely an iron oxide particle. The *in vivo* ability of L-ferritin-M6A to self assemble was further demonstrated using ferritin-knockout HeLa cells transfected with L-ferritin-M6A (Figure S2).[22] Therefore, this extra density is likely an iron oxide formed *in vivo*. However, since ferritins were shown to promote the sedimentation of a wide range of substances, the ability to remove this density by chelation and replace it by a treatment with iron ions had to be confirmed.

In addition to the formation of the biomineral particles, we found that the C-terminus of L-ferritin and part of M6A became

https://dx.doi.org/10.1021/jacs.0c07565
J. Am. Chem. Soc. 2020, 142, 19551−19557

partially structured under these conditions, resulting in the formation of ~2 helix turns in the N-terminal part of M6A. This result agrees with studies of M6A in solution[17] and secondary structure predictions using JPred[23] that show that M6A is unstructured in the context of Mms6 (with a weak tendency of its last two amino acids to form a helix) as well as when it is conjugated to the C-terminus of L-ferritin. When observed at low thresholds, the density of M6A extends and overlaps with the density of the biomineral particle. This finding suggests that M6A's disordered region weakly interacts with the particle and, as a result, has an increased propensity to sample its vicinity. However, these structural changes might result from the fusion of M6A to ferritin or from the interaction with ions inside the ferritin cage, requiring further examination.

To determine whether the extra density found in the untreated sample is an *in vivo*-formed mineral and whether this mineral impacted the M6A folding, the protein was treated with an acetate wash to chelate its metal content, and its structure was determined again by cryo-EM and X-ray crystallography. The extra density found in the untreated protein was absent from the cryo-EM and X-ray crystallography maps (at 3.0 and 1.7 Å resolutions, respectively) of the "acetate-washed" ferritin-M6A (Figures 3 and S3). Therefore, the

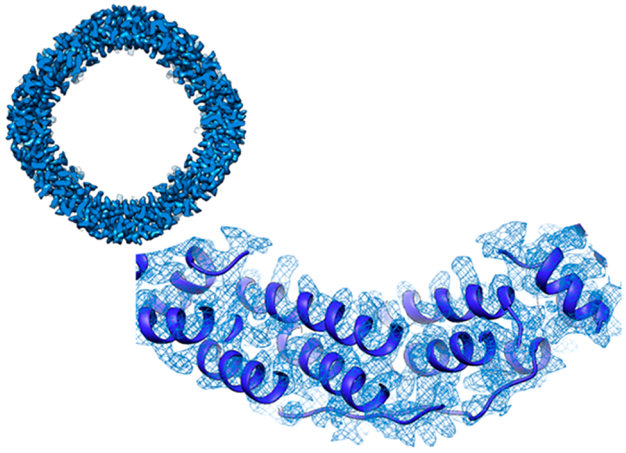

Figure 3. Without mineral particles M6A is unstructured. No sediment densities were found in the map of the acetate-washed protein (top), and the extra helical turn of M6A could not be observed (the ribbon diagram of mouse L-ferritin (PDB 1LB3) is presented to guide the eye).

spherical densities observed in the untreated protein were indeed of biomineral particles. Moreover, the extra helical turns of M6A that were found in the untreated protein were absent in the acetate-washed protein, indicating that the partial stabilization of M6A is correlated with the formation of the biomineral particles and cannot be explained by the scaffolding effect of ferritin.

To control the nature of the sediment, we next introduced iron ions into L-ferritin-M6A by incubating the acetate-washed ferritin cages in a buffer supplemented with $FeCl_2$ to allow for *de novo* iron oxide mineralization inside ferritin-M6A. The $FeCl_2$-treated protein structure ("refilled") was determined by cryo-EM, giving rise to a ~2.7 Å resolution map (PDB 6ZH5). The resulting map had a large additional density protruding from the 4-fold symmetry axes of ferritin that extended along its inner surface toward the 2-fold symmetry axes (Figure 4). The density near the 4-fold axes, which is where M6A starts, clearly appeared as a helix, and spherical features near the 2-fold symmetry axes

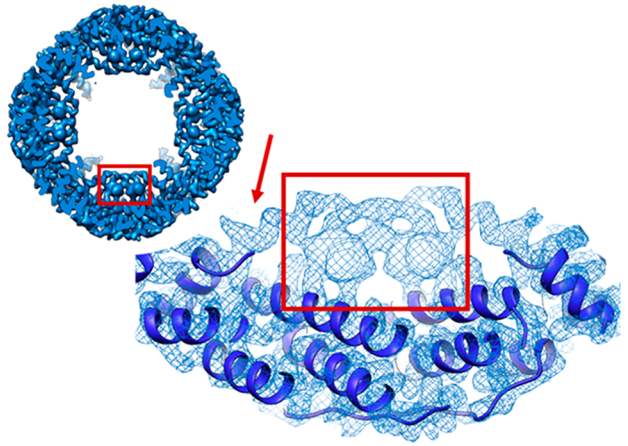

Figure 4. Cryo-EM map of the refilled sample. A cut through the EM density map (top) reveals a large density positioned where the biomineral particles in the untreated samples were found (red box). The density of M6A protrudes from the C-terminal end of ferritin (red arrow) and continues in the vicinity of the iron oxide particles (the ribbon diagram of mouse L-ferritin (PDB 1LB3) is presented to guide the eye).

were likely iron oxide particles. Therefore, some of the structural features of the map could be directly interpreted. However, tracing M6A with an atomic model around the iron oxide particle was challenging due to its irregular shape and close contacts with the protein.

We realized that the differences in the electron-dose sensitivity of the protein and the iron oxide particles could assist in telling the protein apart from the mineral.[25] To distinguish between them, we developed a "radiation damage-assisted single-particle analysis" protocol (the detailed protocol is found in the Supporting Information), which utilizes the differences in the electron-dose sensitivity of the organic and inorganic phases of the structure (Figure 5).[26−28] The 3D map of the refilled sample was reconstructed twice without changing the alignment parameters that were determined during the initial

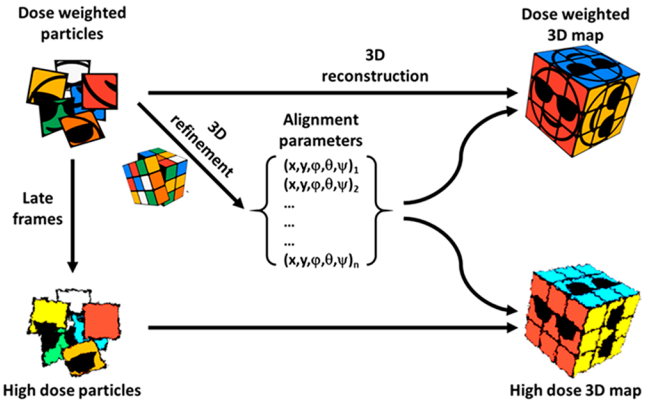

Figure 5. Radiation damage-assisted single-particle analysis. The alignment parameters (shifts and Euler angles) were determined by the 3D refinement of the dose-weighted particles. These parameters are used for reconstituting the "regular" dose-weighted high-resolution map. High-dose (i.e., late frames) sums of the particles were produced from the movies of the same-aligned particles. The high-dose 3D map was reconstructed by applying the reconstruction parameters that were determined for the dose-weighted particles on the high-dose sums of the particles.

https://dx.doi.org/10.1021/jacs.0c07565
J. Am. Chem. Soc. 2020, 142, 19551−19557

dose-weighted refinement. The maps were reconstructed, once using the early frames (0−40 $e^-/Å^2$), and once using the late frames (40−80 $e^-/Å^2$) of each particle. As expected, due to their higher radiation sensitivity the protein chains were diffused and absent in most of the regions of the late-frames map, highlighting the electron densities of the iron oxide particles.

Using a difference map between the low- and high-dose maps to guide the model building, we modeled the structure of most of M6A, revealing its interaction with the forming iron oxide particles. The resulting structure had 12 pairs of almost spherical particles. The particles in each pair were located on both sides of the octahedral ferritin cage 2-fold symmetry axes (Figure 6a).

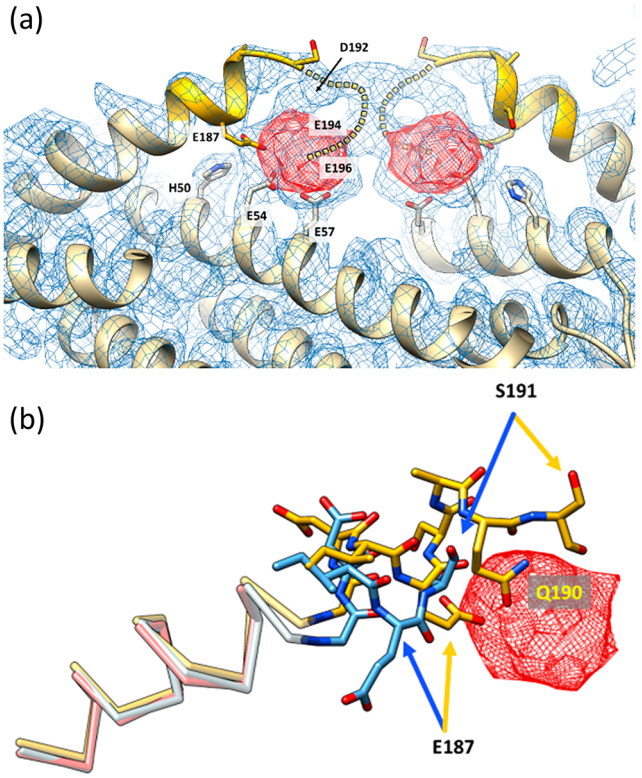

Figure 6. M6A becomes structured in response to the formation of iron oxide particles. (a) The density of a large iron oxide particle (red) was revealed by the radiation damage-assisted single-particle analysis. M6A forms a helix and an extended loop that wraps around the iron oxide particles. (b) Comparison between the atomic models of M6A of the untreated (blue) and refilled (yellow) conditions. The segment of L-ferritin that precedes M6A is presented by washed shades (pink, acetate washed; light blue , untreated; and light yellow, refilled). Note the change in the orientations of Glu187 and Ser191.

The iron oxide particles were considerably larger (~225 $Å^3$, fitting 10−13 iron ions) than the iron oxide clusters previously found in wild type (wt) L-ferritin.[4] The interaction with M6A shifted the iron oxide particle by one α-helix turn away from the wt iron nucleation site, located near the middle of the second helix of L-ferritin.[5] Hence, out of the four negatively charged amino acids that coordinate the Fe ions in wt-L-ferritin (E54, E57, E58, and E61), only two are in contact with the M6A-stabilized iron oxide particle (E54 and E57). M6A becomes partially structured when it interacts with the iron oxide particle and wraps around it. This M6A conformation consists of a helix followed by an extended loop. We could not fully trace M6A's C-terminus due to possible flexibility in the vicinity of the particle, which limited the accurate assignment of these residues. Nevertheless, the density of the loop was clearly apparent. The M6A helix interacts with the iron oxide particle through its glutamate 187 (E187) amino acid, and the loop interacts with the particle through its aspartate 192 amino acid and two glutamates, 194 and 196 (i.e., E118, D123, E125, and E127 in the Mms6 sequence, respectively) (Figure 6b). Most of the interactions with the iron oxide particle are mediated by the loop, either by transient interactions, as found in the untreated sample, or by more stable interactions in the refilled sample. Therefore, the stabilization of the helix is nonlocal, where interactions with the iron oxide particle in the C-terminal part of M6A induce a conformational change of its N-terminal part.

DISCUSSION

In this work, we followed the structural changes of M6A in response to the formation of iron oxide particles in its vicinity. The structure determination of biomineralization proteins while in complex with minerals is challenging due to incompatibilities between structural methods and the conditions required for the formation of these complexes. For example, growing sediments of more than a few ions while maintaining intact protein crystals is challenging and limits high-resolution X-ray crystallography studies. Similarly, biomineralization proteins tend to form nonuniform and nonstoichiometric higher-order structures when interacting with protein−mineral complexes.[7] These diverse morphologies, which are typical to biomineralization processes, are incompatible with sample preparation and image analysis methods used in high-resolution cryo-EM studies. Conjugating M6A to the C-terminus of L-ferritin allowed us to circumvent these obstacles.

Ferritins are oligomeric proteins with a cage-like structure, which perform iron binding and storage functions in numerous organisms. Their ability to sequester metals has inspired many nanotechnological studies aimed at utilizing ferritin as a platform for MRI applications, controlled drug release, the leaching of ions from the environment, and as an artificial mineralization tool.[19,29,30] Here, we used ferritin as a scaffold for positioning M6A near an artificially nucleated iron oxide nanoparticle, and tested their interactions. To control the direct effect of the inner surface of L-ferritin on the structure of M6A, we solved the structure of L-ferritin-M6A without sediment precipitates (the acetate-washed sample) by cryo-EM and X-ray crystallography. In both structures (Figures 3 and S3), the density of M6A was absent, confirming that it was unstructured under these conditions as expected from secondary structure predictions and previous studies.[15−17] Because ferritin and its mutants can recruit a wide range of metals, we expect that this strategy will be applicable for a wide range of systems, especially ones that bind divalent cations.

To analyze our results, we developed an image processing protocol for assisting the molecular model building in cases where the protein−nanomineral interface is hard to discern in the density maps. Using this method, we determined the structure of the M6A/iron oxide particle complex formed by incubating L-ferritin-M6A in an $FeCl_2$-supplemented buffer. Under these conditions, a relatively large iron oxide particle was formed (10−13 Fe ions). More than half of the particle's surface area is in contact with M6A, indicating strong binding. Most of the interactions between the M6A and the iron oxide particle are mediated by negatively charged amino acids, suggesting that the particle's surface is positively charged.

https://dx.doi.org/10.1021/jacs.0c07565
J. Am. Chem. Soc. 2020, 142, 19551−19557

A comparison between the untreated and the refilled structures shows that when the iron oxide particle is larger, M6A is more structured. This result may explain previous observations of the effect of magnetite on the structure of Mms6 and the finding that Mms6 facilitates the early stages of sediment formation.[12] However, in contrast with its *in vivo* function, the iron oxide particles in our study are likely not magnetite. Consequently, the interaction between M6A and the iron oxide particle seems to be nonspecific. This result is in line with other studies, which demonstrated the ability of IDPs to interact with substrates in a nonspecific manner.[8]

The conformational changes of M6A demonstrate that proteins that are in direct contact with the forming biominerals can sense and respond to the geometry of the minerals. The C-terminal loop of M6A becomes more localized due to its multiple interactions with the iron oxide particle. In contrast, the N-terminal segment, which does not interact with the particle in the untreated sample and has only a limited interaction with the particle in the refilled sample, is stabilized and forms a helix. The stabilization of this helix can be explained by classical biophysical helix−coil transition models[31] that capture the cooperative nature of the helix formation. Under such a scheme, the partial localization of the C-terminal loop can lead to the stabilization of a helix away from the particle, therefore propagating a signal from the C-terminal to the N-terminal side of M6A. Highly charged intrinsically unstructured regions are found in many biomineralization proteins.[5] Therefore, it is likely that a similar effect can be found in other biomineralization systems.

The response of M6A to the sediments can function as a mechanism for controlling the microstructure. The interaction of the C-terminal region of M6A with the iron oxide particle can directly affect its geometry by dynamically altering its surface energy and the diffusion rate of ions. Alternatively, the stabilization of the helix at the N-terminal side of M6A due to the interactions of its C-terminal loop with the iron oxide particle may act like a sensor that mediates the modulation of other parts of the biomineralization machinery. This observation suggests an extension of the fly casting model[32] to a "fly-sensing" scenario where transient cues at the contact site with the sediment are transmitted to the rest of the protein.

MATERIALS AND METHODS

Protein Expression and Purification. The gene encoding the ferritin light chain 1 (Ftl1) and the magnetite biomineralization protein Mms6 Asp116−Glu127 was synthesized in a frame with Gly as a linker between the two proteins and subcloned into a pET28a *Escherichia coli* expression vector (Novagen) between the NdeI and *Bam*HI restriction sites. In this construct, a 6-His tag was fused at the L-ferritin-M6A N-terminus with a thrombin cleavage site (done by Biomatik©, Cambridge, Ontario N3H4R7, Canada).

For protein expression, the plasmid was introduced into *E. coli* BL21 strain cells in a Luria broth (LB) medium containing kanamycin (100 mg/mL) at 37 °C and 180 rpm. Protein overexpression was induced by the addition of isopropyl-D-thiogalactopyranoside (IPTG) to a final concentration of 0.3 mM when the cell culture reached an optical density of 0.6 at 600 nm. After induction, cells were allowed to grow for an additional 16 h at 20 °C and 180 rpm. The cells were harvested by centrifugation (8000 × *g*) for 25 min at 4 °C. Cells were resuspended in a lysis buffer (20 mM Tris-HCl pH 8, 200 mM ammonium sulfate, 20 mM imidazole, 10% glycerol, and 2 mM tris(2-carboxyethyl)phosphine hydrochloride (TCEP)) and incubated with DNase I (10 mg/mL) and a protease inhibitor cocktail (100 mM phenylmethylsulfonyl fluoride (PMSF), 1.2 mg/mL leupeptin, and 1 mM pepstatin A) at a ratio of 1:1000 with the binding buffer for 20 min at 4 °C, followed by either disruption by two cycles in a French press pressure cell at 207 MPa or homogenization (C5 homogenizer, Avestin). Cell debris were separated by centrifugation at 19 000 *g* for 60 min at 15 °C. L-Ferritin-M6A was purified from the supernatant fraction by a homemade gravity Ni-NTA column (2.5 cm diameter, Econo-Column Chromatography Columns, Bio-Rad; Ni-NTA His Bind Resin; Lot no. M0063428, Novagen) equilibrated with lysis buffer. The protein was washed with two different wash buffers, wash buffer I (20 mM Tris-HCl pH 8, 500 mM ammonium sulfate, 40 mM imidazole, 10% glycerol, and 2 mM TCEP) and wash buffer II (20 mM Tris-HCl pH 8, 200 mM ammonium sulfate, 20 mM imidazole, 10% glycerol, and 2 mM TCEPs). Elution was performed using an elution buffer (20 mM Tris-HCl pH 8, 200 mM ammonium sulfate, 5% glycerol, 2 mM TCEP, and 50 mM ethylenediaminetetraacetic acid (EDTA)). The eluted protein was concentrated, and the buffer was replaced with the SEC buffer (see below) and further concentrated using an Amicon Ultra filtration unit 10 000 MWCO (Millipore Sigma, Darmstadt, Germany). Several SEC buffers were tested to obtain the assembled nanocage L-ferritin-M6A. The final SEC buffer was 20 mM Bis-Tris pH 5.8, 500 mM KCl, and 10% glycerol. The L-ferritin-M6A was applied to a column of HiLoad 26/60 Superdex 200 (GE Healthcare Biosciences) equilibrated with the SEC buffer (Figure S1). The purified nanocage L-ferritin-M6A was then concentrated to 15−20 mg/mL, flash-frozen in liquid nitrogen, and stored at −80 °C. The protein concentration was determined by UV absorbance at a wavelength of 280 nm using a molar extension coefficient of 12 950 $(M{\cdot}cm)^{-1}$. The final protein purity was determined by SDS−PAGE and Coomassie staining to be around 95% (Figure S1).

L-ferritin-M6A without the His tag (L-ferritin-M6A-H) was purified as described with an additional step of thrombin cleavage. Bovine thrombin (10 U/ml; 9002−04−4, Fisher Bioreagents) was added to the L-ferritin-M6A protein washed with the SEC buffer for 16 h under rotation at 20 °C.

Preparation of Proteins at Different Iron-Loading States. Proteins for cryo-EM imaging were prepared in the following three different states: (I) purified nanocage L-ferritin-M6A ("untreated"), (II) purified nanocage L-ferritin-M6A after a sodium acetate treatment ("acetate-washed"), and (III) purified nanocage L-ferritin-M6A after a sodium acetate treatment followed by iron loading ("refilled"). To ensure that the imaging of all three states was performed under the same conditions, the last step prior to the plunge freezing of cryo-EM samples was the transfer, by dialysis of 16 h at 20 °C, of the protein into a cryo-EM imaging buffer (20 mM Bis-Tris pH 5.8, 500 mM KCl, and 0.5% glycerol), followed by the dilution of the protein to 0.1 mg/mL.

The acetate-washed protein was prepared by diluting the purified nanocage L-ferritin-M6A (i.e., the untreated protein) to 10 mg/mL in the SEC buffer and supplementing the sample with 0.5 M sodium acetate buffer, resulting in final concentrations of 0.25 M sodium acetate at pH 4.6 and 5 mg/mL protein, followed by incubation for 6−8 h.

The refilled protein was prepared by transferring the acetate-washed protein at a concentration of 5 mg/mL by dialysis back to the SEC buffer, followed by a further dilution of the protein to 0.1 mg/mL and incubation in the SEC buffer supplemented with $FeCl_2$ to a final concentration of 0.044 mM $FeCl_2$. The 1 mM $FeCl_2$ stock solution used in this experiment was freshly prepared by adding $FeCl_2$ (F1632161 113 MERCK, Darmstadt, Germany) to the N_2-purged SEC buffer.

X-ray Crystallography. Purified L-ferritin-M6A and L-ferritin-M6A-His were crystallized by the sitting-drop vapor diffusion method at 20 °C. To form the drop, 0.5 μL of protein was mixed with 0.5 μL reservoir solutions. The crystallization trials were performed with L-ferritin-M6A or L-ferritin-M6A-H concentrated from 2 to 15 mg/mL at 20 °C in the SEC buffer. The initial crystallization conditions were examined using commercial screening kits from Hampton Research (Index) and Molecular Dimensions (structure screen I + II HT), and many conditions were scanned without data collection. The finest crystal appeared after 3 months in a well containing L-ferritin-M6A-H (15 mg/mL) in structure screen conditions no. 4 (0.1 M sodium acetate pH 4.6 and 2 M sodium formate). Details of X-ray crystallography data collection and analysis are provided in the Supporting Information.

https://dx.doi.org/10.1021/jacs.0c07565
J. Am. Chem. Soc. 2020, 142, 19551−19557

Cryo-EM. Cryo-EM samples were prepared by plunge freezing into liquid ethane. The protein solution (2.5−3 μL) at a concentration of 0.1 mg/mL was deposited on glow-discharged Quantifoil R1.2/1.3 holey carbon grids (Quantifoil Micro Tools GmbH, Germany), and the sample was manually blotted for 4 s and vitrified by rapidly plunging it into liquid ethane using a home-built plunging apparatus. The frozen samples were stored in liquid nitrogen until imaging.

Samples were loaded under cryogenic conditions and imaged under low-dose conditions on a Tecnai F30 Polara microscope (FEI, Eindhoven) operated at 300 kV. Data sets were collected with SerialEM[33] using a homemade automated data collection script.[34] Imaging was done by a K2 Summit direct electron detector fitted behind an energy filter (Gatan Quantum GIF) set to ±10 eV around the zero-loss peak. The calibrated pixel size at the sample plane was 1.1 Å. The detector was operated in a dose fractionated counting mode at a dose rate of ∼8 e^-/pixel/s. Each dose-fractionated movie had 50 frames, with a total electron dose of 80 $e^-/Å^2$. Data was collected at a defocus range from −1.0 to −2.5 μm.

Dose-fractionated image stacks were aligned using MotionCorr2,[35] and their defocus values were estimated by Gctf.[36] The sum of the aligned frames was used for further processing by Relion3.0.[37] Particles were autopicked based on a template produced from a small subset of manually picked particles. The picked particles were processed by an *ab initio* 2D classification, followed by a manual inspection and the selection of the class averages. Classes were selected based on the shape and number of particles. All selected classes had clear signatures of secondary structure elements. The initial 3D reference was prepared from the data set of the untreated sample. Final maps were obtained by 3D refinement, imposing an octahedral (O) symmetry. The resolution was assessed by Fouriers shell correlation. The different stages of image processing of each EM structure are summarized in Figures S4−S6 and Table S2.

While the results presented here were obtained by assuming an octahedral symmetry, reprocessing the data with no symmetry assumption gave similar results (EMD-11365). Thus, in the case of the refilled map, while we cannot rule out some variability between the iron oxide particles, our results suggest that they are the same.

■ ASSOCIATED CONTENT

Supporting Information

The Supporting Information is available free of charge at https://pubs.acs.org/doi/10.1021/jacs.0c07565.

SEC profile of L-ferritin-M6A, cell cultures, iron recruitment experiments, detailed description of crystallography and cryo-EM data collection, processing and validation, and a detailed protocol for the radiation damage analysis (PDF)

Description of Movie S1 (PDF)

Movie showing the maps (MPG)

■ AUTHOR INFORMATION

Corresponding Author

Gabriel A. Frank − *Department of Life Sciences and The National Institute for Biotechnology in the Negev, Ben-Gurion University of the Negev, Beer Sheva 8410501, Israel;* orcid.org/0000-0001-8379-5133; Email: frankg@bgu.ac.il

Authors

Geula Davidov − *Department of Life Sciences and The National Institute for Biotechnology in the Negev, Ben-Gurion University of the Negev, Beer Sheva 8410501, Israel*

Gili Abelya − *Department of Life Sciences, Ben-Gurion University of the Negev, Beer Sheva 8410501, Israel*

Ran Zalk − *The National Institute for Biotechnology in the Negev, Ben-Gurion University of the Negev, Beer Sheva 8410501, Israel*

Benjamin Izbicki − *Department of Life Sciences, Ben-Gurion University of the Negev, Beer Sheva 8410501, Israel*

Sharon Shaibi − *Department of Life Sciences, Ben-Gurion University of the Negev, Beer Sheva 8410501, Israel*

Lior Spektor − *Faculty of Biotechnology and Food Engineering, Technion−Israel Institute of Technology, Haifa 3200000, Israel*

Dayana Shagidov − *Faculty of Biotechnology and Food Engineering, Technion−Israel Institute of Technology, Haifa 3200000, Israel*

Esther G. Meyron-Holtz − *Faculty of Biotechnology and Food Engineering, Technion−Israel Institute of Technology, Haifa 3200000, Israel*

Raz Zarivach − *Department of Life Sciences, The National Institute for Biotechnology in the Negev, and Ilse Katz Institute for Nanoscale Science and Technology, Ben-Gurion University of the Negev, Beer Sheva 8410501, Israel;* orcid.org/0000-0001-6543-0296

Complete contact information is available at: https://pubs.acs.org/10.1021/jacs.0c07565

Author Contributions

⊥These authors contributed equally.

Notes

The authors declare no competing financial interest.

■ ACKNOWLEDGMENTS

This study was supported by the Israeli Ministry of Science and Technology Grants for R.Z. and G.A.F (Italy−Israel Scientific and Technological Cooperation Grant 3-14335) and the Israel Science Foundation (Grant 515/2018 to E.G.M.-H.). The authors wish to thank Mr. Yehuda Barouch for IT support, and Prof. Anat Ben-Zvi for constructive criticism of the manuscript.

■ REFERENCES

(1) Moura, H. M.; Unterlass, M. M. Biogenic Metal Oxides. *Biomimetics* **2020**, *5*, 29.

(2) Sharma, V.; Srinivasan, A.; Nikolajeff, F.; Kumar, S. Biomineralization process in hard tissues: The interaction complexity within protein and inorganic counterparts. *Acta Biomater.* **2020**, DOI: 10.1016/j.actbio.2020.04.049.

(3) Hoang, Q. Q.; Sicheri, F.; Howard, A. J.; Yang, D. S. C. Bone recognition mechanism of porcine osteocalcin from crystal structure. *Nature* **2003**, *425*, 977−980.

(4) Ciambellotti, S.; Pozzi, C.; Mangani, S.; Turano, P. Iron Biomineral Growth from the Initial Nucleation Seed in L-Ferritin. *Chem. - Eur. J.* **2020**, *26*, 5770−5773.

(5) Pozzi, C.; Ciambellotti, S.; Bernacchioni, C.; Di Pisa, F.; Mangani, S.; Turano, P. Chemistry at the protein-mineral interface in L-ferritin assists the assembly of a functional (μ3-oxo)Tris[(μ2-peroxo)] triiron(III) cluster. *Proc. Natl. Acad. Sci. U. S. A.* **2017**, *114*, 2580−2585.

(6) Kalmar, L.; Homola, D.; Varga, G.; Tompa, P. Structural disorder in proteins brings order to crystal growth in biomineralization. *Bone.* **2012**, *51*, 528−534.

(7) Boskey, A. L.; Villarreal-Ramirez, E. Intrinsically disordered proteins and biomineralization. *Matrix Biol.* **2016**, *52*−*54*, 43−59.

(8) Vacic, V.; Oldfield, C. J.; Mohan, A.; Radivojac, P.; Cortese, M. S.; Uversky, V. N.; Dunker, A. K. Characterization of molecular recognition features, MoRFs, and their binding partners. *J. Proteome Res.* **2007**, *6*, 2351−2366.

(9) Arachchige, R. J.; Burton, S. D.; Lu, J. X.; Ginovska, B.; Harding, L. K.; Taylor, M. E.; Tao, J.; Dohnalkova, A.; Tarasevich, B. J.; Buchko, G. W.; Shaw, W. J. Solid-State NMR Identification of Intermolecular Interactions in Amelogenin Bound to Hydroxyapatite. *Biophys. J.* **2018**, *115*, 1666−1672.
(10) Villarreal-Ramirez, E.; Eliezer, D.; Garduño-Juarez, R.; Gericke, A.; Perez-Aguilar, J. M.; Boskey, A. Phosphorylation regulates the secondary structure and function of dentin phosphoprotein peptides. *Bone.* **2017**, *95*, 65−75.
(11) Arakaki, A.; Masuda, F.; Amemiya, Y.; Tanaka, T.; Matsunaga, T. Control of the morphology and size of magnetite particles with peptides mimicking the Mms6 protein from magnetotactic bacteria. *J. Colloid Interface Sci.* **2010**, *343*, 65−70.
(12) Tanaka, M.; Mazuyama, E.; Arakaki, A.; Matsunaga, T. MMS6 protein regulates crystal morphology during nano-sized magnetite biomineralization in vivo. *J. Biol. Chem.* **2011**, *286*, 6386−6392.
(13) Wang, L.; Prozorov, T.; Palo, P. E.; Liu, X.; Vaknin, D.; Prozorov, R.; Mallapragada, S.; Nilsen-Hamilton, M. Self-assembly and biphasic iron-binding characteristics of Mms6, a bacterial protein that promotes the formation of superparamagnetic magnetite nanoparticles of uniform size and shape. *Biomacromolecules* **2012**, *13*, 98−105.
(14) Zhang, H.; Liu, X.; Feng, S.; Wang, W.; Schmidt-Rohr, K.; Akinc, M.; Nilsen-Hamilton, M.; Vaknin, D.; Mallapragada, S. Morphological transformations in the magnetite biomineralizing protein Mms6 in iron solutions: A small-angle X-ray scattering study. *Langmuir* **2015**, *31*, 2818−2825.
(15) Rawlings, A. E.; Bramble, J. P.; Hounslow, A. M.; Williamson, M. P.; Monnington, A. E.; Cooke, D. J.; Staniland, S. S. Ferrous Iron Binding Key to Mms6Magnetite Biomineralisation: A Mechanistic Study to Understand Magnetite Formation Using pH Titration and NMR Spectroscopy. *Chem. - Eur. J.* **2016**, *22*, 7885−7894.
(16) Rawlings, A.E.; Liravi, P.; Corbett, S.; Holehouse, A.S.; Staniland, S.S. Investigating the ferric ion binding site of magnetite biomineralisation protein Mms6. *PLoS One* **2020**, *15*, e0228708.
(17) Nudelman, H.; Lee, Y.Z.; Hung, Y.L.; Kolusheva, S.; Upcher, A.; Chen, Y.C.; Chen, J.Y.; Sue, S.C.; Zarivach, R. Understanding the biomineralization role of magnetite-interacting components (MICs) from magnetotactic bacteria. *Front. Microbiol.* **2018**, *9*, 02480 DOI: 10.3389/fmicb.2018.02480.
(18) Feng, S.; Wang, L.; Palo, P.; Liu, X.; Mallapragada, S. K.; Nilsen-Hamilton, M. Integrated self-assembly of the Mms6 magnetosome protein to form an Iron-responsive structure. *Int. J. Mol. Sci.* **2013**, *14*, 14594−14606.
(19) Liang, M.; Fan, K.; Zhou, M.; Duan, D.; Zheng, J.; Yang, D.; Feng, J.; Yan, X. H-ferritin-nanocaged doxorubicin nanoparticles specifically target and kill tumors with a single-dose injection. *Proc. Natl. Acad. Sci. U. S. A.* **2014**, *111*, 14900−14905.
(20) Radoul, M.; Lewin, L.; Cohen, B.; Oren, R.; Popov, S.; Davidov, G.; Vandsburger, M. H.; Harmelin, A.; Bitton, R.; Greneche, J.-M.; Neeman, M.; Zarivach, R. Genetic manipulation of iron biomineralization enhances MR relaxivity in a ferritin-M6A chimeric complex. *Sci. Rep.* **2016**, *6*, 26550.
(21) Russo, C. J.; Passmore, L. A. Ultrastable gold substrates for electron cryomicroscopy. *Science (Washington, DC, U. S.)* **2014**, *346*, 1377−1380.
(22) Truman-Rosentsvit, M.; Berenbaum, D.; Spektor, L.; Cohen, L. A.; Belizowsky-Moshe, S.; Lifshitz, L.; Ma, J.; Li, W.; Kesselman, E.; Abutbul-Ionita, I.; Danino, D.; Gutierrez, L.; Li, H.; Li, K.; Lou, H.; Regoni, M.; Poli, M.; Glaser, F.; Rouault, T. A.; Meyron-Holtz, E. G. Ferritin is secreted via 2 distinct nonclassical vesicular pathways. *Blood* **2018**, *131*, 342−352.
(23) Drozdetskiy, A.; Cole, C.; Procter, J.; Barton, G. J. JPred4: a protein secondary structure prediction server. *Nucleic Acids Res.* **2015**, *43*, 389−394.
(24) Granier, T.; Langlois D'Estaintot, B.; Gallois, B.; Chevalier, J. M.; Précigoux, G.; Santambrogio, P.; Arosio, P. Structural description of the active sites of mouse L-chain ferritin at 1.2 Åresolution. *JBIC, J. Biol. Inorg. Chem.* **2003**, *8*, 105−111.
(25) Martynowycz, M. W.; Hattne, J.; Gonen, T. Experimental Phasing of MicroED Data Using Radiation Damage. *Structure* **2020**, *28*, 458−464 e2.
(26) Grant, T.; Grigorieff, N. Measuring the optimal exposure for single particle cryo-EM using a 2.6 Åreconstruction of rotavirus VP6. *eLife* **2015**, *4*, No. 06980.
(27) Baker, L. A.; Rubinstein, J. L., Radiation Damage in Electron Cryomicroscopy. In *Cryo-EM Part A Sample Preparation and Data Collection*; Jensen, G. J., Ed.; Methods in Enzymology, Vol *481*; Elsevier Inc.,: San Diego, CA, 2010; pp 371−388. DOI: 10.1016/S0076-6879(10)81015-8.
(28) Hattne, J.; Shi, D.; Glynn, C.; Zee, C.-T.; Gallagher-Jones, M.; Martynowycz, M. W.; Rodriguez, J. A.; Gonen, T. Analysis of Global and Site-Specific Radiation Damage in Cryo-EM. *Structure* **2018**, *26*, 759−766.
(29) Cohen, B.; Dafni, H.; Meir, G.; Harmelin, A.; Neeman, M. Ferritin as an endogenous MRI reporter for noninvasive imaging of gene expression in C6 glioma tumors. *Neoplasia.* **2005**, *7*, 109−117.
(30) He, D.; Marles-Wright, J. Ferritin family proteins and their use in bionanotechnology. *New Biotechnol.* **2015**, *32*, 651−657.
(31) Lifson, S.; Roig, A. On the theory of helix-coil transition in polypeptides. *J. Chem. Phys.* **1961**, *34*, 1963−1974.
(32) Shoemaker, B. A.; Portman, J. J.; Wolynes, P. G. Speeding molecular recognition by using the folding funnel: The fly-casting mechanism. *Proc. Natl. Acad. Sci. U. S. A.* **2000**, *97*, 8868−8873.
(33) Mastronarde, D. N. Automated electron microscope tomography using robust prediction of specimen movements. *J. Struct. Biol.* **2005**, *152*, 36−51.
(34) Frank, G.A. Serial EM script. *The Frank Group: Connecting Structure and Function.* https://www.frank-cryoem.com/resources.
(35) Zheng, S. Q.; Palovcak, E.; Armache, J. P.; Verba, K. A.; Cheng, Y.; Agard, D. A. MotionCor2: Anisotropic correction of beam-induced motion for improved cryo-electron microscopy. *Nat. Methods* **2017**, *14*, 331−332.
(36) Zhang, K. Gctf: Real-time CTF determination and correction. *J. Struct. Biol.* **2016**, *193*, 1−12.
(37) Zivanov, J.; Nakane, T.; Forsberg, B.O.; Kimanius, D.; Hagen, W.J.; Lindahl, E.; Scheres, S.H. New tools for automated high-resolution cryo-EM structure determination in RELION-3. *eLife* **2018**, *7*, No. e42166, DOI: 10.7554/eLife.42166.

https://dx.doi.org/10.1021/jacs.0c07565
J. Am. Chem. Soc. 2020, 142, 19551−19557